Journal of Alloys and Compounds 485 (2009) 853–861

Contents lists available at ScienceDirect

Journal of Alloys and Compounds

journal homepage: www.elsevier.com/locate/jallcom

Fracture mechanism and strength-influencing factors of Cu/Sn–4Ag solder joints aged for different times

Q.K. Zhang, Z.F. Zhang*

Shenyang National Laboratory for Materials Science, Institute of Metal Research, Chinese Academy of Sciences, Shenyang 110016, PR China

ARTICLE INFO

Article history:
Received 5 March 2009
Received in revised form 16 June 2009
Accepted 17 June 2009
Available online 23 June 2009

Keywords:
Sn–4Ag solder
Interfacial IMCs
Tensile properties
Strain rate
Fracture mechanism

ABSTRACT

Tensile properties and fracture mechanisms of Cu/Sn–4Ag solder joints aged at 180 °C for different times were investigated at the strain rates of $1.25 \times 10^{-4}\,s^{-1}$ and $1.25 \times 10^{-1}\,s^{-1}$. At the low strain rate, it was found that the tensile strength of the solder joints decreased with increasing aging time in principle, though the tendency was not monotonously at the early stage of aging; and all the solder joints had similar tensile curves but different fracture morphologies and fracture processes. At the high strain rate, tensile strength of the solder joints was much higher and decreased monotonously with increasing aging time, with identical fracture process and fractographies. Evolution of the Cu/Sn–4Ag interfacial morphology during aging process and the effect of aging on tensile property of the Sn–4Ag alloy were also involved for further analysis. Based on the experimental results and observations, the fracture processes were revealed and some factors controlling the tensile strength of solder joints were discussed qualitatively.

1. Introduction

Because the toxicity of Pb element in conventional Sn–37Pb solder presents a major health hazard, many lead-free solder alloys have been proposed as alternatives in electronic package. Since the solders used in electronic packaging field serve not only to provide the electronic connection but also to ensure the mechanical reliability of solder joints under the service conditions [1], it has been recognized that one of the major concerns for the integrity of the solder interconnection is the strength and damage mechanisms at the solder/substrate interfaces under various practical service conditions.

In recent years, there have been many investigations on various series of lead-free solder joints from this viewpoint [2–8], while tensile behaviors of as-soldered and isothermal aged solder joints were widely investigated. It has been reported that tensile strength of the Cu/lead-free solder joints decreased with increasing interfacial IMC thickness in principle and crack usually occurred at the Cu/solder interface [2–6]. Nevertheless, most of these studies only involved the experiments performed to evaluate the tensile strength of the solder joints; only a few reports are concerning the fracture mechanisms. Lee et al. [3] suggested that the fracture mechanism of the Sn–Ag/Cu solder joints changed from dimple-ductile fracture to transcrystalline-brittle fracture with increasing IMC thickness at the strain rate of about $2 \times 10^{-4}\,s^{-1}$. Kikuchi et al. [9] reported that the as-soldered Sn–Ag/Cu solder joints exhibited a dimple-ductile fracture with a high elongation at the strain rate of $8.3 \times 10^{-4}\,s^{-1}$. However, both of the fracture mechanisms were simply predicated based on only some special region of fracture surfaces. In addition, effect of tensile strain rate on adhesive strength of the solder joints has also been investigated [4,9]. It has been recognized that the tensile strength increased with increasing strain rate, but influence of strain rate on fracture mechanism of solder joints was less informed. Meanwhile, although influence of aging on mechanical properties of the lead-free solder has been reported [10–12], its effect on the adhesive strength of solder joints was not ever proposed. The evolution regularity of the tensile strength of solder joints with increasing aging time was not well explained, too.

The discussion above indicates that a comprehensive understanding on fracture mechanism of the solder joints and a conclusion of strength-influencing factors are required. In this study, the Cu/Sn–4Ag solder joints were used; tensile fracture behaviors of the solder joints aged for different times were investigated. The aging time was chosen with a short time step to better reveal the evolution of interfacial morphology and transition of fracture mechanism during aging process. In addition, effect of strain rate on deformation and fracture behaviors of the solder joint was also considered for comparison. By comprehensively comparing and analyzing the fracture surfaces of solder joints, both the intrinsic and the external factors influencing tensile strength were considered to understand the fracture mechanism. Furthermore, it is expected that the current research will provide a new understanding on fracture mechanism of the lead-free solder joints.

* Corresponding author. Tel.: +86 24 23971043.
E-mail address: zhfzhang@imr.ac.cn (Z.F. Zhang).

0925-8388/$ – see front matter © 2009 Elsevier B.V. All rights reserved.
doi:10.1016/j.jallcom.2009.06.108

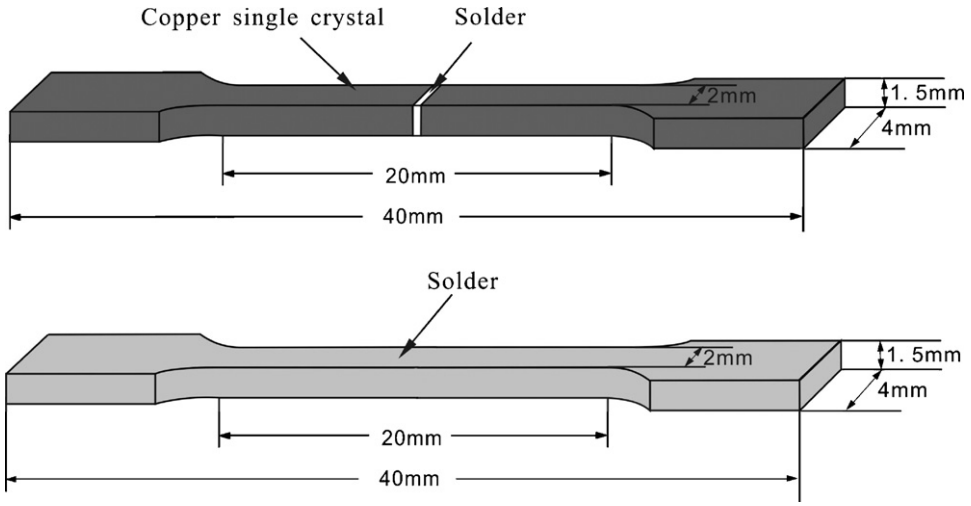

Fig. 1. Illustration of tensile samples of solder joints and bulk solder alloy.

2. Experimental procedures

As the most widely used substrate material in electronic package and scientific experiment, Cu was chosen as substrate, prepared from oxygen-free-high conductivity (OFHC) Cu of 99.999% purity by the Bridgman method in a horizontal furnace, in this study. Moreover, the Sn–Ag alloy is considered as one of the most potential lead-free solder candidates for its well soldering ability and excellent mechanical properties [1,13,14], thus, Sn–4Ag (wt%) solder, prepared by melting high purity (>99.99%) tin and silver in vacuum at 800 °C for 30 min, was used in the present work. The microstructure of slow-cooling Sn–4Ag alloy is composed of proeutectic plate-like Ag_3Sn intermetallics and a eutectic structure of Sn and needle-like Ag_3Sn particles [11].

The Cu plate was firstly spark-cut into blocks and the ends to be soldered were carefully polished with a diamond polishing agent for the final solder. Before reflowing, a soldering paste was dispersed on the selected area of the polished Cu surface, an Sn–4Ag alloy sheet was placed on the paste to ensure sufficient wetting reaction. Graphite plates were clamped on the sides of the Cu samples with the solder paste to avoid the outflow of the molten solder. These prepared samples were fixed in an oven with a constant temperature of 260 °C for 10 min to evaporate the rosin flux and then were cooled down in air. Selected samples were isothermally aged at 180 °C for 4, 16, 36, 64, 100, 225 and 400 h in air atmosphere, respectively. After that, the as-soldered and aged samples were spark-cut into miniature specimens comparable in size to actual solder joints in electronic packaging, as illustrate in Fig. 1. Then the side surfaces were ground and carefully polished for observations of the microstructures and deformation morphologies of the Cu/Sn–4Ag interfaces. Furthermore, in order to reveal the effect of aging on tensile strength solder; air-cooled Sn–4Ag alloy plate was cut into samples with the same size as the solder joints and then aged at 180 °C.

Tensile tests were performed with an Instron E1000 fatigue testing machine with the maximum static load of 710 N at room temperature in air. The tensile strain rates were chosen to be $1.25 \times 10^{-4}\ s^{-1}$ and $1.25 \times 10^{-1}\ s^{-1}$, respectively. Tensile tests of solder specimens were performed only at the strain rate of $1.25 \times 10^{-4}\ s^{-1}$, and at least three tensile tests were performed on each sample condition to substantiate the reproducibility of the stress–strain curves. The microstructure of the Cu/Sn–4Ag interfacial features and fracture surfaces of the solder joints were characterized to reveal the growth kinetics of IMC layer, the deformation and fracture morphologies of samples in a LEO SUPRA35 field emission scanning electronic microscope (SEM) with energy dispersive X-ray (EDX) spectroscopy.

3. Results and discussion

3.1. Evolution of interfacial morphology

Fig. 2 shows the microscopic morphologies of the as-soldered and aged Sn–4Ag/Cu interfaces. For the as-soldered interface, an IMC layer with scallop-like morphology was formed along the

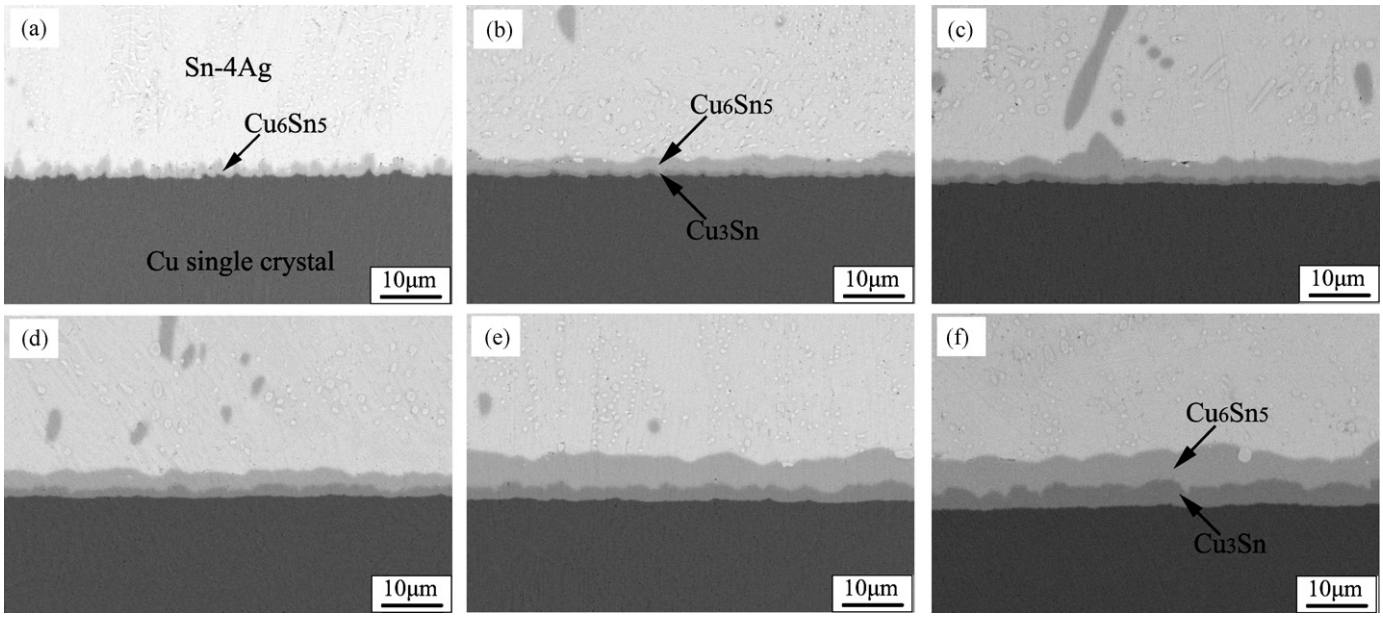

Fig. 2. Interfacial morphologies of (a) as-soldered sample and samples aged at 180 °C for: (b) 4 h, (c) 16 h, (d) 36 h, (c) 100 h and (f) 400 h.

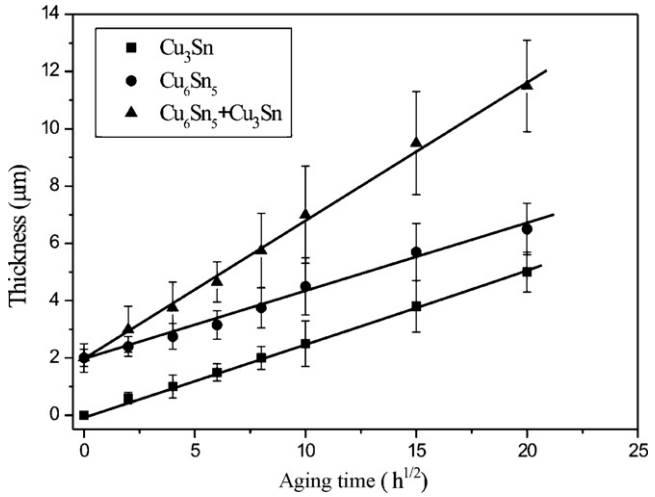

Fig. 3. Dependence of interfacial IMC thickness of the Cu/Sn–4Ag solder joints on aging time at 180 °C.

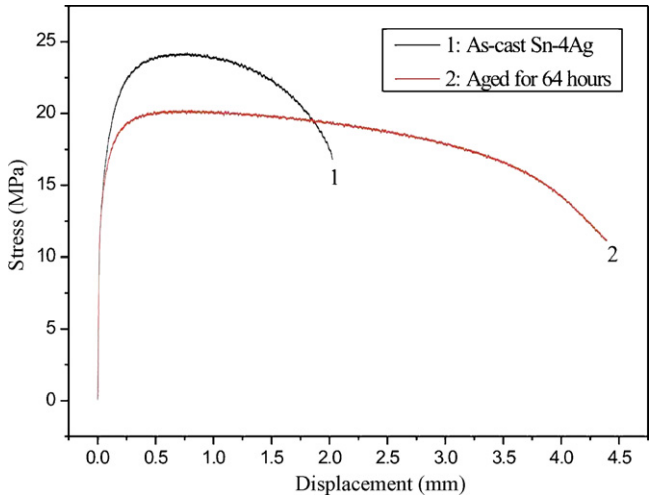

Fig. 4. Uniaxial stress–displacement curves of Sn–4Ag solder alloy aged for different times at the strain rate of $1.25 \times 10^{-4}\ s^{-1}$.

interface, as shown in Fig. 2(a). EDX analysis indicates that the IMC layer with average thickness of ~2 μm is the Cu_6Sn_5 phase. After isothermally aging at 180 °C for 4 h, the IMC/solder interface became evidently flat (see Fig. 2(b)). Meanwhile, careful examination on the interface revealed that the scallop-type Cu_6Sn_5 layer was changed to planar-type duplex layers of IMCs. The new interfacial IMC phase, identified to be Cu_3Sn phase, is more obvious in Fig. 2(c). It has been reported that both of the two IMCs are very brittle and can significantly influence the interfacial tensile properties [10,15–19]. It is obvious that the growth of the IMCs should be faster in the valleys of the scallop than in the peaks during the flattening process since the growth of the IMCs is controlled by the grain boundary diffusion mechanism and the valleys of the IMC layer always correspond to the grain boundaries [6,15,16]. During the later aging process, the IMC layer kept increasing and the Cu_6Sn_5 phase near the IMC/Cu interface was transformed into Cu_3Sn phase, as shown in Fig. 2(c–f). The top surface of the Cu_6Sn_5 layer is always rough, but there is no obvious roughness of the Cu_6Sn_5/Cu_3Sn and the solder/Cu_6Sn_5 interfaces even after aging for 400 h.

Compared to the microstructure of the as-cast (see Fig. 2(a)) and aged solder shown in Fig. 2(b–f), a coarsening trend of the needle-like Ag_3Sn particles was observed, which may in turn affect the mechanical properties of the solder alloy [11]. However, the difference in microstructures of the aged solder alloy is not significant because the grain of the air-cooled solder alloy is already very coarse. Further coarsening during aging process, which may occur only at the early stage, should be not very remarkable. Thus, the microstructures of the long-term aged solder alloy are stable.

In this study, the thickness of the IMC layers measured from the SEM images was calculated by using the following equation:

$$\delta = \frac{S}{L} \tag{1}$$

where L is the length of the measured region, S is the integral contour area of the IMC at the interface, and δ is the average thickness of the IMC layer. The IMC thickness of a sample is the mean value of the IMC thickness at different places of the interface, which reflects the whole growth trend of the IMC layer. As exhibited in Fig. 3, the IMC thicknesses are approximately proportional to the square root of aging time at 180 °C. Based on the diffusion mechanism controlling the growth process of the IMC layers during aging processes [17–19], early investigations indicated that the growth of Cu–Sn IMCs can be expressed by the following one-dimensional empirical equation:

$$\delta = \delta_0 + \sqrt{Dt}, \tag{2}$$

where δ and δ_0 are the thicknesses of IMC at time t and zero, D is the diffusion coefficient and t is the aging time. The value of the diffusion coefficient D at 180 °C was calculated as $7.78 \times 10^{-17}\ m^2 s^{-1}$ for the whole Cu_6Sn_5/Cu_3Sn layer by measuring their thicknesses at different aging times. This is approximately equal to the previous results of the polycrystalline Cu/SnAgCu interface, i.e. $8.1 \times 10^{-17}\ m^2 s^{-1}$ at 190 °C and single crystal Cu/SnAgCu interface, i.e. $7.24 \times 10^{-17}\ m^2 s^{-1}$ at 170 °C and single crystal Cu/SnAg interface, i.e. $7.82 \times 10^{-17}\ m^2 s^{-1}$ at 180 °C [20–22].

3.2. Influence of aging on tensile properties of Sn–4Ag solders

The typical nominal stress–displacement curves of the Sn–4Ag solder at the strain rate of $1.25 \times 10^{-4}\ s^{-1}$ are illustrated in Fig. 4. It was found that the tensile properties of the solder were apparently influenced by the aging treatment, resulting in a decrease in the offset yield strength ($\sigma_{0.2}$) and an increase in elongation. This is attributable to the coarsening and dispersion of the Ag_3Sn as well as the coarsening of the solder grain induced by isothermal aging [6,10–12]. However, the decrease of strength is slight and the trend becomes inconspicuous with increasing aging time. The small difference in the yield strength of the aged samples, as shown in Fig. 5, is in accord with the foresaid microstructure observations. In addition, the strain to failure of the aged samples significantly increases, while the difference in elongation of the samples aged for different times is not very remarkable.

As shown in Fig. 4, both the as-cast and the aged Sn–4Ag solders exhibit very low work-hardening rates. Therefore, the stress–displacement curves exhibit a plateau or even slightly descend, indicating that creep plays an important role in the plastic deformation of solder. It has been acknowledged that the tensile property of the Sn-based solder is substantially influenced by the strain rate and temperature: an increase in strain rate or decrease in temperature results in an increase in strength [13,23–28]. Generally, the relationship between the tensile strength of solder and the strain rate can be expressed by a power type equation like high-temperature creep [23–29]:

$$\sigma = C\dot{\varepsilon}^m. \tag{3}$$

where σ is the tensile strength, $\dot{\varepsilon}$ is the strain rate, m is the strain rate sensitivity and C is a constant. It has been measured that the

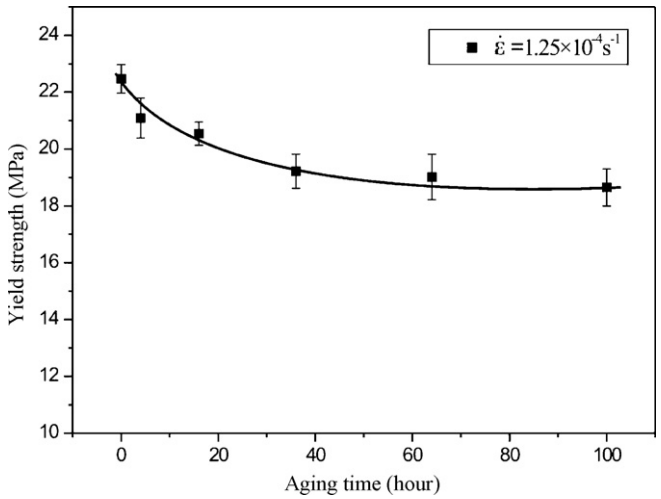

Fig. 5. Dependence of yield strength of the Sn–4Ag solder on the aging time.

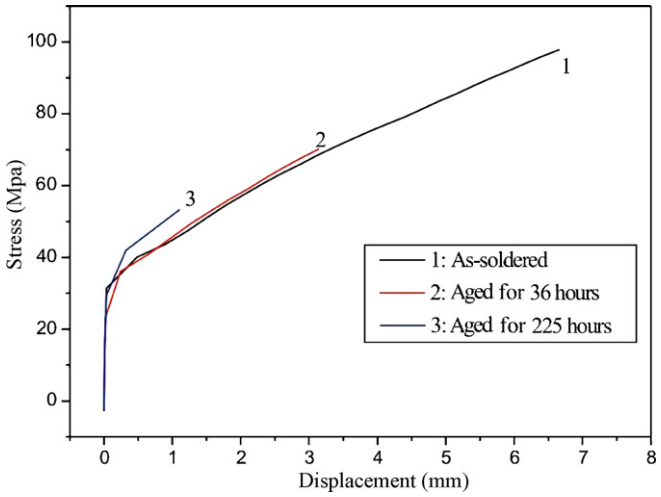

Fig. 7. Uniaxial stress–displacement curves of solder joints aged for different times at the strain rate of 1.25×10^{-1} s^{-1}.

values m of the Sn–Ag and SnAgCu alloy are about 0.08 [13,30]. Consequently, one could expect that the tensile strength of the Sn–4Ag solder at the strain rate of 1.25×10^{-1} s^{-1} is about 1.74 times higher than that at the strain rate of 1.25×10^{-4} s^{-1}. In addition, when the strain is very high, the strength of solder will keep steady with increasing strain rate [25,31]. Influence of strain rate on the strength of solders may in turn affect the adhesive strength of solder joints, making it higher at high strain rate, which will be discussed later in this paper.

3.3. Tensile strength of solder joints aged for different times

The dependence of tensile strength (σ_b) on aging time at two different strain rates is demonstrated in Fig. 6. It is notable that at the strain rate of 1.25×10^{-1} s^{-1}, the tensile strength represents a rapid decrease when aging at the first few hours, which may be attributed to the decrease in the strength of solder. Then it decreases approximately linear with increasing aging time. That is to say, it also decreases with increasing interfacial IMCs thickness. In contrast, at the strain rate of 1.25×10^{-4} s^{-1}, evolution of the tensile strength is a little complex. According to some previous reports [3,4], although the tensile strength decreases with increasing aging time in principle, the tendency is not monotonously. In addition, it can be seen from Fig. 6 that the tensile strength at the strain rate of

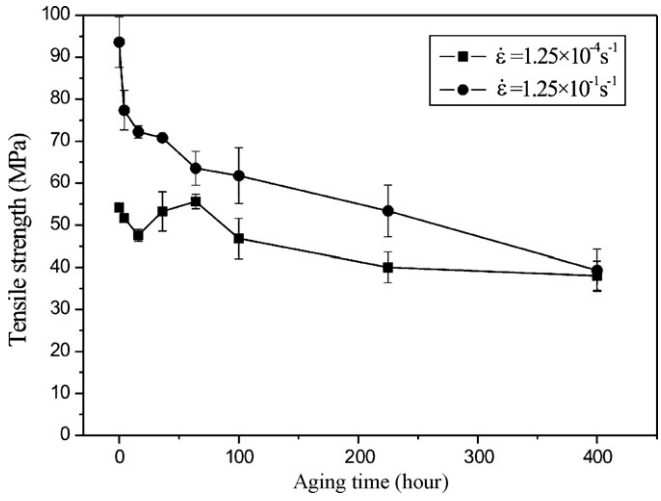

Fig. 6. Tensile strength of solder joints aged for different times at two different strain rates.

1.25×10^{-1} s^{-1} is much higher than that at 1.25×10^{-4} s^{-1}, but the difference reduces with increasing aging time, indicating that the fracture mechanisms of the long-term aged solder joints may be similar. Thus, it is very essential to characterize the side surfaces and fracture morphologies of the samples to reveal the fracture processes and the influencing factors on the adhesive strength.

It has been reported that the tensile strength increases with increasing strain rate and their relationship also obeys Eq. (3) and the values m are in the range of 0.1–0.25 for all the solders [9]. Thus, it is predicated that creep deformation of solder during tensile test plays a crucial role in the plastic deformation of solder joints. Naturally, when the strain rate is very high, the creep of solder will be restrained completely. Theoretically, the differential function of Eq. (3) can be expressed as below:

$$d\sigma/d\dot{\varepsilon} = mC\dot{\varepsilon}^{m-1} \tag{4}$$

From Eq. (4), it can be seen that when the strain rate is very high, the slope of the $\sigma - \dot{\varepsilon}$ curve will be close to zero, implying that the tensile strength will approach to a steady value. This fits well with our former prediction and is also well consistent with the relationship between the strain rate and strength of solder alloys discussed before.

3.4. Tensile fracture behaviors of the solder joints at high strain rate

Fig. 7 exhibits the nominal stress–displacement curves of solder joints tested at the strain rate of 1.25×10^{-1} s^{-1}. It is noted that all the stress–displacement curves, which are similar, show three stages, i.e. elastic deformation, plastic flow with obvious strain-hardening and at last, a sudden final fracture. After elastic deformation, yield appears at the stress of 35 MPa, then the flow stress increases with increasing displacement in an approximately linear manner. According to the similarity of the slope of the curves, the strain hardening rates should also be similar. However, for the solder joints aged for different times, not only the plastic strains but also tensile strengths are significantly different. Although the plastic strains are considerable, necking was not observed from the curves. In contrast, the samples failed in a brittle mode, which will be further discussed based on the observations of the fracture surfaces.

In order to demonstrate the fracture mechanism, the macroscopic and microscopic fracture morphologies of the solder joints tested at the strain rate of 1.25×10^{-1} s^{-1} are carefully charac-

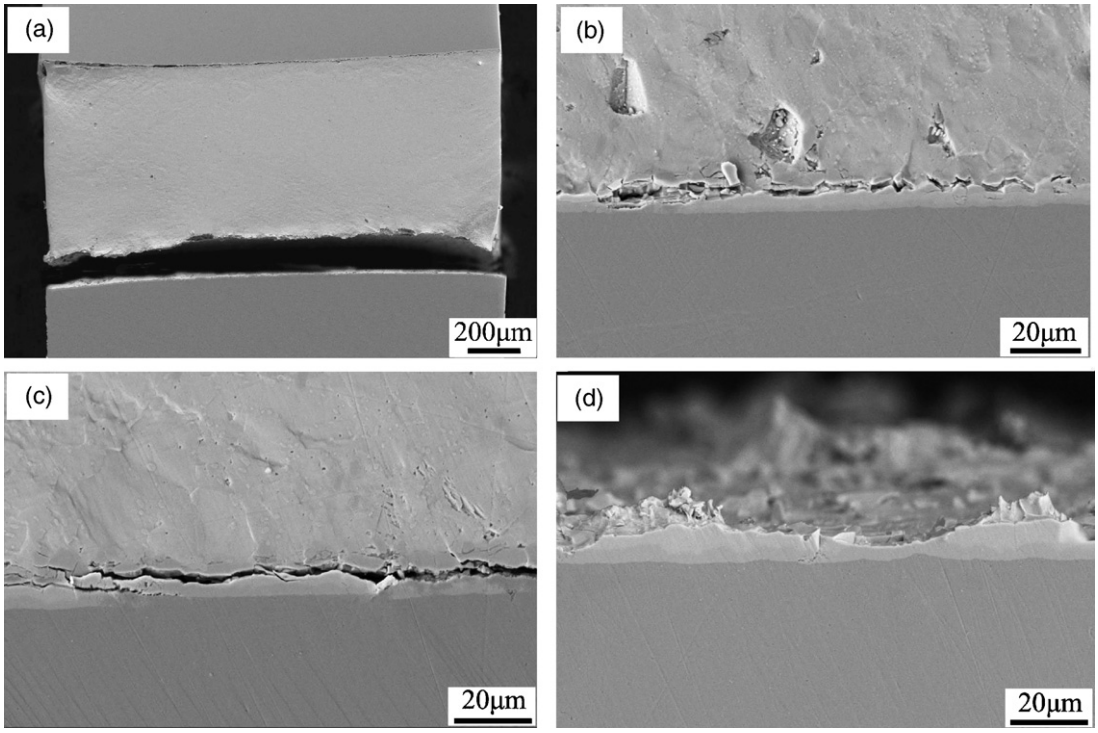

Fig. 8. Side surfaces morphologies of solder joints at the strain rate of $1.25 \times 10^{-1}\ s^{-1}$ (a) macroscopic image of fracture sample aged for 100 h; (b) interfacial micrograms of solder joints aged for 36 h (c) 100 h and (d) 225 h.

terized. As illustrated in Fig. 8(a), no severe macroscopic plastic deformation of the solder aged for 100 h was observed, This phenomena may be ascribed to the high strain rate and the short tensile time (1 s or so) by considering the sensitivity of strength on the time-dependent plastic deformation [13,24–29]. It seems that interfacial hardening, appeared at the Cu/solder interface, induces a "knuckle-like" shape, which may cause stress concentration at the interface, especially at the brim of sample. Fig. 8(b–d) show the microscopic features on the side surfaces of the cracked solder joints aged for 36, 100, and 225 h, respectively. Apparently, the side surfaces of specimens aged for different times are quite similar; i.e. cracking occurred inside the interfacial IMCs although the interfacial IMC thickness is different. In addition, the fracture location of the long-term aged samples is more close to the Cu/Cu_3Sn interface. The macroscopic fracture surfaces of the solder joints aged for 0, 16 and 400 h are shown in Fig. 9(a–c), it is obvious that all the surfaces are quite flat, and only difference in the sizes of IMC grains induces different roughness in appearance. Fig. 9(d–f) show the corresponding microscopic fracture morphologies. The fracture surfaces are covered by the cracked IMCs. A spot of streaky struc-

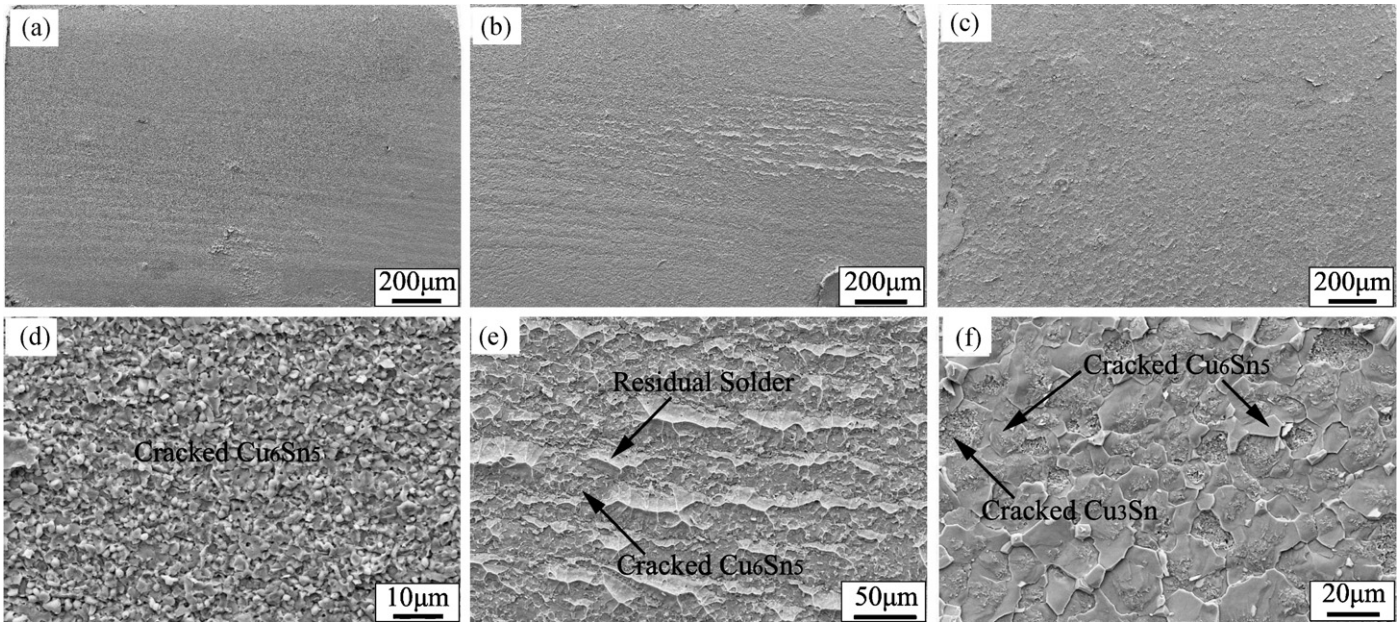

Fig. 9. Fracture surfaces morphologies of solder joints at the strain rate of $1.25 \times 10^{-1}\ s^{-1}$: (a) macroscopic image of as-soldered sample and (b) samples aged for 16 h and (c) 400 h; (d) microscopic image of as-soldered sample and (e) samples aged for 16 h and (f) 400 h.

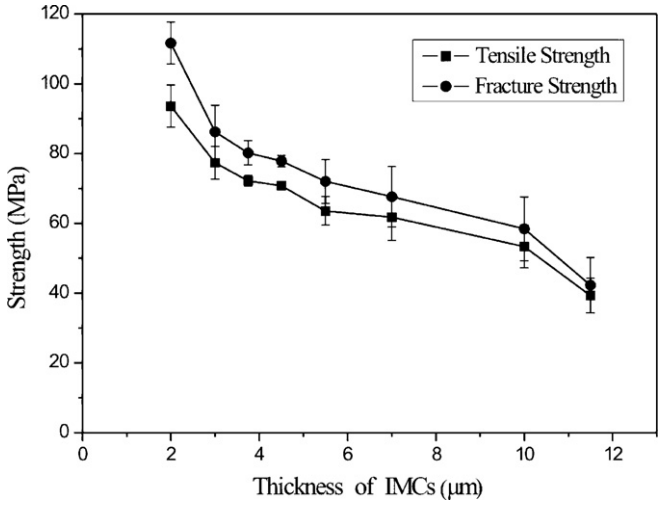

Fig. 10. Dependence of the tensile strength and fracture strength on the aging time for the solder joints tested at the strain rate of $1.25 \times 10^{-1}\ s^{-1}$.

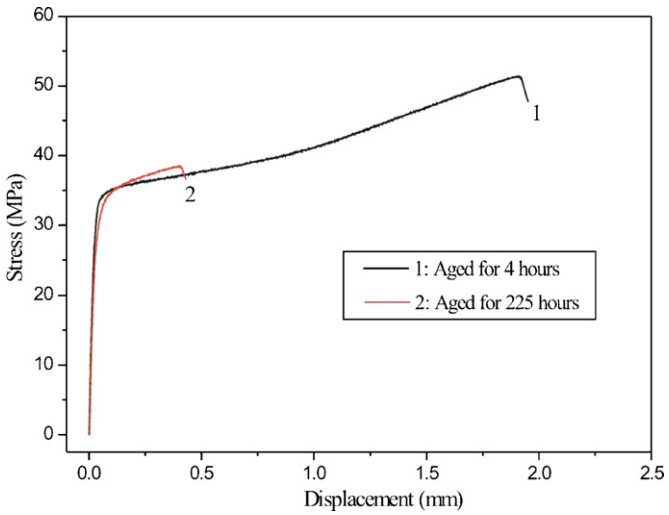

Fig. 11. Uniaxial stress–displacement curves of solder joints aged for different times at the strain rate of $1.25 \times 10^{-4}\ s^{-1}$.

ture was observed in some specimens, as shown in Fig. 9(e). For the fracture surfaces aged for over 100 h, not only Cu_6Sn_5 but also Cu_3Sn was cracked (see Fig. 9(f)). In general, the cross-sections of the samples are well consistent with the images of the side surfaces and the normal stress–displacement curves. It confirms that all the solder joints represent a brittle fracture in an inter-granular mode.

Previous discussion has revealed that when the strain rate is very high, the tensile strength of solder joints will approach to a steady value. In fact, since the interfacial IMCs are too brittle to show any plastic deformation, the strain rate has little effect on the elastic deformation and the brittle fracture process. When the strain rate is high enough to restrain the creep of solder, the tensile strength will not increase any more. Observations of the side surfaces (see Fig. 8) have approved that the creep of solder was restrained at the strain rate of $1.25 \times 10^{-1}\ s^{-1}$ and fracture occurred inside the interfacial IMCs. Therefore, it is reasonable to predicate that the tensile strength has approached to the maximum value, defined as the "intrinsic adhesive strength" in this paper. Fig. 10 shows the fracture strength (σ_f) of the solder joints at the strain rate of $1.25 \times 10^{-1}\ s^{-1}$, which was taken for the approximate value of the intrinsic adhesive strength and as the sufficient condition of the final fracture. Since all the samples cracked in the same mode and the fracture strength decreases monotonously with increasing IMC thickness, the tendency may be attributed to an intrinsic property of the interfacial IMCs. Other researchers have reported that severe residual transition stress is accumulated in the interior of the interfacial IMCs during its growth process [32,33], which makes the IMCs more brittle and decreases its intrinsic adhesive strength.

3.5. *Tensile fracture behaviors of the solder joints at low strain rate*

Fig. 11 shows two nominal stress–displacement curves of the solder joints at the strain rate of $1.25 \times 10^{-4}\ s^{-1}$. There are also three stages: elastic deformation, plastic flow with obvious strain-hardening and final fracture after a slight necking. Similar to the curves shown in Fig. 7, the elastic strain is very little and the yield strength is about 35 MPa (see curves in Fig. 11). The flow stress also increases after yielding, but the strain-hardening rate changes with increasing strain and is much lower than that shown in Fig. 7. Besides, the plastic strains and tensile strengths of the solder joints aged for different times are quite different. Another notable difference is that necking is observed in the curves, as observed in Fig. 11, indicating that the samples may fail in a ductile mode.

The macroscopic deformation behavior of solder joints at the strain rate of $1.25 \times 10^{-4}\ s^{-1}$ is exhibited in Fig. 12. Compared to the image shown in Fig. 8 (a), the plastic strain and necking of solder joints are obviously remarkable. The strain localization induced by deformation incompatibility was observed at the brim of the solder/Cu interface, which in turn induces severe shear stress at the brim of samples. Fracture occurred mainly at the solder/Cu interface; sometimes the cracks may propagate into the solder and induce a shear fracture.

In general, two different fracture surfaces of samples aged for different times are revealed at the strain rate of $1.25 \times 10^{-4}\ s^{-1}$. Typical fracture morphologies of the solder joints, whose tress-displacement curves are presented in Fig. 11, are shown in Figs. 13 and 14. For the first type, in macro-scale, three regions were observed in the sample aged for 4 h, as exhibited in Fig. 13 (a). The first region with the elongated dimples along a trace of shear stress is covered by deformed solder and the major axis of the dimples is parallel to the shear direction (see Fig. 13 (b)). Similar images were also observed at the shear fracture surface of the solder joints [6,7,34,35]. Thus, the first region is induced by the shear stress. The second region, similar to the image in Fig. 9(e), is composed of the interlaced residual solder and cracked IMCs, as shown in Fig. 13(c). The third region, exactly the same as the typical fracture morpholo-

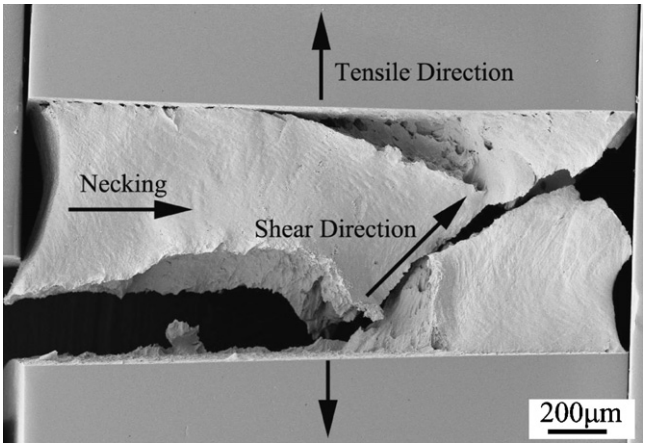

Fig. 12. Macroscopic image of cracked solder joints tested at the strain rate of $1.25 \times 10^{-4}\ s^{-1}$.

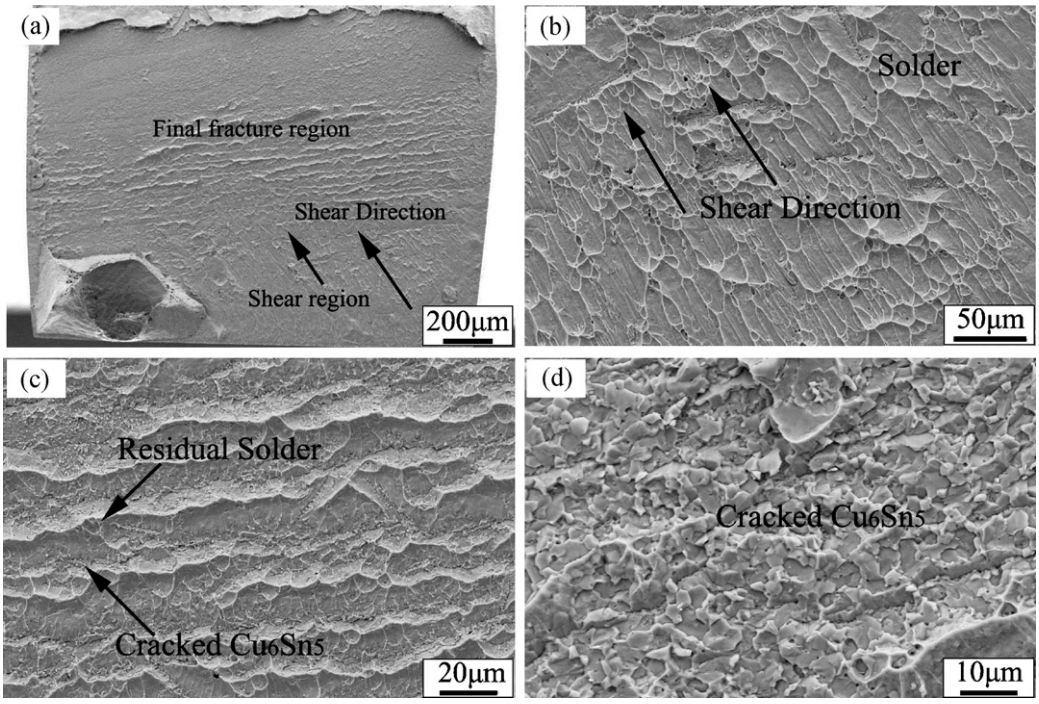

Fig. 13. Fracture surfaces of solder joint aged for 4 h at the strain rate of 1.25×10^{-4} s^{-1}: (a) macroscopic image; (b) fracture morphologies of shear region; (c) streaky structure and (d) inter-granular brittle fracture region.

gies at the high strain rate (see Fig. 13(d)), is covered by cracked IMCs. Compared to Fig. 9, it can be concluded that both the second and third regions are formed at high strain rate; namely, in the final fracture process. Thus, the two regions make up of the final fracture region.

Another representative fracture surface is shown in Fig. 14, in which the sample was aged for 225 h. Compared to the image shown in Fig. 13(a), the fracture surface of the long-term aged solder joints is relatively simple (see Fig. 14(a)), and the shear fracture region was not observed. Indeed, the plastic strain of the solder joint during tensile test is very small (see curve 2 in Fig. 11), which corresponds well with the fracture surface. Fig. 14 (b) shows the micrograph of the side surface at the edge of the specimen. The microscopic fracture surfaces, illustrated in Fig. 14(c) and (d), show that almost the whole fracture surface is covered by cracked IMCs, Cu_6Sn_5 or Cu_3Sn. Combined with Fig. 14 (b), it is reasonable to conclude that the solder joint cracked in a transcrystalline mode. Nevertheless, obvious shear lip observed at the brim of cracked samples, may

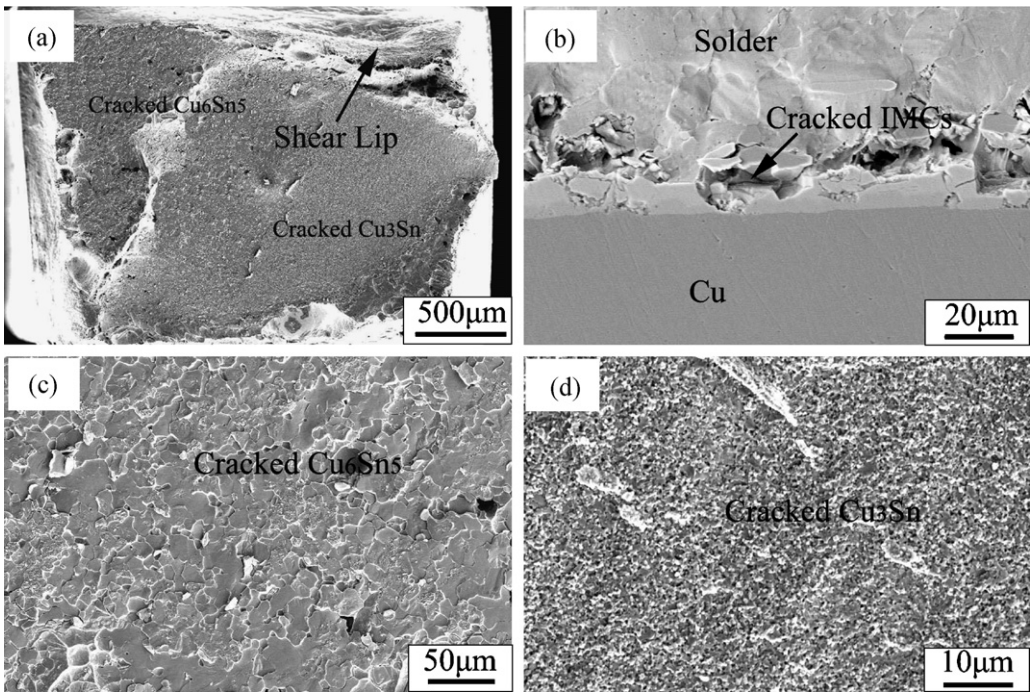

Fig. 14. Fracture surfaces morphologies of solder joints aged for 225 h at the strain rate of 1.25×10^{-4} s^{-1}:(a) macroscopic image of cross-section and (b) side surface; (c) and (d) microscopic fracture morphologies of the inter-granular brittle fracture region.

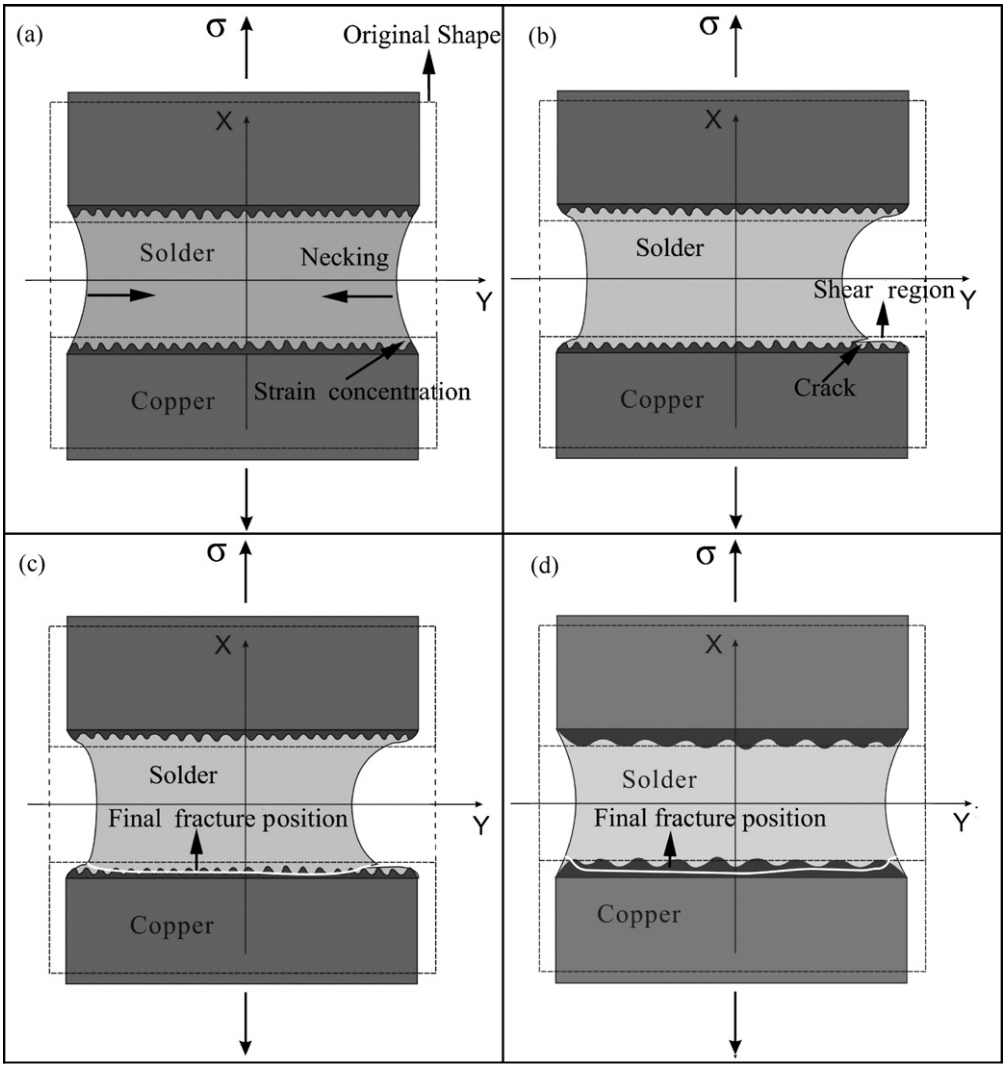

Fig. 15. Illustration of the fracture processes of solder joints at low strain rate: (a) plastic strain incompatibility and necking of solder; (b) shear fracture inside the solder near the solder/Cu_6Sn_5 interface; (c) final brittle fracture in an inter-granular mode; (d) brittle fracture without shear fracture at the interface.

signal that there is still certain plastic deformation of the solder prior to the brittle fracture.

3.6. Fracture process and influencing factors on tensile strength

Based on the experimental observations and discussion above, the tensile facture processes of the Sn–4Ag/Cu solder joints at low strain rate ($1.25 \times 10^{-4}\ s^{-1}$) is described in Fig. 15. For short-term aged solder joints (less than 100 h), the fracture process can be divided into three stages. Firstly, once the solder joint deforms, the solder instantly displays a local necking due to deformation localization, resulting in a local shear stress at the edge of the solder/IMC interface (see Fig. 15(a)). Then the shear stress increases continually with increasing plastic strain. When the shear stress reaches a critical value, the solder close to the solder/IMC interface forms original cracks, as shown in Fig. 15(b). After that, the cracks propagate inside the solder, resulting in a rapid increase in the true stress. Both the initiation and propagation processes of the cracks are affected by the plastic deformation and creep properties of solder. When the true stress reaches to the "intrinsic adhesive strength", the solder joints fail in an inter-granular mode (see Fig. 15(c)). In contrast, for the long-term aged (more than 100 h) samples, the IMC layer is thick and brittle. Though similar phenomenon in Fig. 15(a) also appears, the solder joint will fracture within the interfacial IMCs before the shear fracture of the interfacial solder, as shown in Fig. 15(d). The "final fracture stress" of samples at the strain rate of $1.25 \times 10^{-4}\ s^{-1}$, defined as the ratio of final tensile force to the area of final fracture region, is calculated to confirm the aforesaid prediction. As demonstrated in Fig. 16, the final fracture stress of samples at the strain rate of $1.25 \times 10^{-4}\ s^{-1}$ is quite similar to that of samples at the strain rate of $1.25 \times 10^{-1}\ s^{-1}$. This also indicates that the final fracture occurred at nearly the same true stress, independent of the strain rate, which may be an evidence for the former prediction of the fracture process.

According to the analysis of fracture processes, it can be concluded that there are two governing factors on the tensile strength of solder joints. The first one is the strain rate, which affects the strength of solder joints through its influence on the plastic deformation behaviors (especially creep) of the solder. The relationship between the tensile strength of solder and the strain rate can be expressed by a power–law equation (Eq. (3)) like high-temperature creep at low strain rate. The second dominant factor is the interfacial IMC thickness. When the strain rate is high enough to restrain the creep deformation of solder (for example, $1.25 \times 10^{-1}\ s^{-1}$), the IMC thickness becomes the only controlling factor. As discussed above, the "intrinsic adhesive strength" is governed only by the IMC thickness. Thus, strength of solder joints decreases monotonously with increasing the IMC thickness (see Fig. 10).

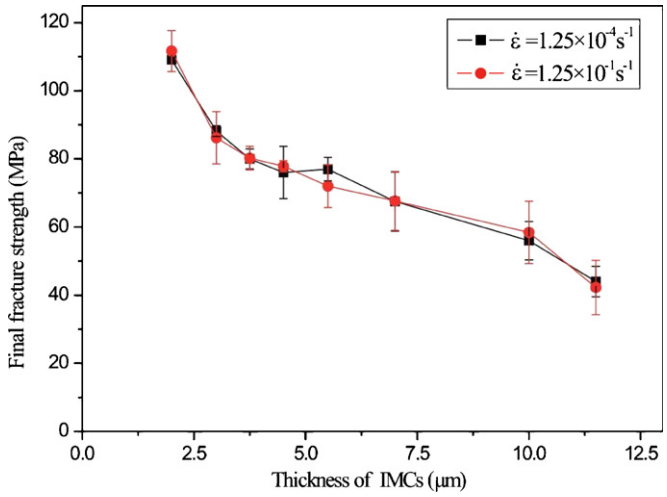

Fig. 16. Final fracture strength of solder joints aged for different times at two strain rates.

However, the tensile strength-aging time curve (see Fig. 6) at the strain rate of $1.25 \times 10^{-4}\,s^{-1}$ is complicated at the early aging stage, indicating that the tensile strength is affected by various factors in this stage. In the early stage of aging, the IMC layer is thin and not too brittle. According to the discussions above, the variation of strength, ductility and creep properties of solder and the roughness of interfacial IMCs during aging process can be main factors influencing the tensile strength. For example, since the aged solder has better ductility, shear fracture does not readily appear in the aged samples than in the as-soldered ones. Besides, the decrease in the strength of solder in this stage will surely decrease the tensile strength, while the evident flatting of interfacial IMCs at the first few hours of aging may raise it. Thus, these different factors make evolution of the tensile strength complicated. In the later stage, the tensile property of solder tends to be stable and the IMC thickness becomes the only dominating factor, so the strength decreases monotonously. Since all Cu/Sn-base solder interfaces have similar evolution process during thermal aging, it can be predicated that similar phenomena could be observed on some other Cu/Sn-base solder interfaces. In fact, many studies have reported the complex evolution processes of the tensile strength of solder joints in the early stage of aging [2–5], which may largely support our predication.

4. Conclusions

Tensile behaviors of Cu/Sn–4Ag solder joints aged at 180 °C for different times and tested at the strain rates of $1.25 \times 10^{-1}\,s^{-1}$ and $1.25 \times 10^{-4}\,s^{-1}$ were investigated. Based on the experimental results and analysis, the following conclusions can be drawn:

(1) Due to coarsening of the eutectic structure and the needle-like Ag_3Sn particles during early aging process, tensile strength of the aged Sn–4Ag solder is relatively lower than that of the as-cast one, while the elongation is significantly improved. However, the tensile properties of solders aged for different times shows little difference.
(2) The tensile strength of solder joints at the strain rate of $1.25 \times 10^{-1}\,s^{-1}$ is higher than that at the strain rate of $1.25 \times 10^{-4}\,s^{-1}$, but the difference reduces with increasing aging time. This implies that the tensile strength increases with increasing strain rate but tends to be stable if the strain rate is high enough to restrain the creep of solder.
(3) For the short-term aged solder joints, there is severe plastic strain incompatibility and strain concentration at the brim of sample during tensile test, necking of solder induces a shear stress at the interface. Cracking initiates inside the solders close to the solder/IMC interface and propagates along the interface driven by the shear stress. When the true normal stress is up to the fracture strength, final brittle fracture occurs. The long-term aged samples or samples test at high strain rate exhibit similar brittle fracture in an inter-granular mode.
(4) Strain rate is the dominant external factor and the interfacial IMC thickness is the predominant internal factor on tensile strength of solder joints. At high strain rate the interfacial IMC thickness is the decisive factor and the others can be neglected. At low strain rate, the variation of strength, ductility and creep properties of solder during aging process and roughness of the interfacial IMCs could be main factors, making the tensile strength-aging time curve complex, in the early aging stage. However, the IMC thickness becomes the dominating factor at the later stage.

Acknowledgements

The authors would like to acknowledge X.H.An, H.F. Zou, Q.Q. Duan, Q.S. Zhu, P. Zhang, X.X. Zhang, and W. Gao for sample preparation, tensile tests and SEM observations. This work was financially supported by National Basic Research Program of China under grant No. 2004CB619306, the National Natural Science Foundation of China (NSFC) under grant No. 50625103.

References

[1] M. Abtew, G. Selvaduray, Mater. Sci. Eng. R 27 (2000) 95–141.
[2] H.T. Lee, Y.H. Lee, Mater. Sci. Eng. A 419 (2006) 172–180.
[3] H.T. Lee, M.H. Chen, H.M. Jao, T.L. Liao, Mater. Sci. Eng. A 358 (2003) 134–141.
[4] H.F. Zou, Q.S. Zhu, Z.F. Zhang, J. Alloys Compd. 461 (2008) 410–417.
[5] M.S. Suh, C.J. Park, H.S. Kwon, Mater. Chem. Phys. 110 (2008) 95–99.
[6] X. Deng, R.S. Sidhu, P. Johnson, N. Chawla, Metall. Trans. A 36 (2005) 55–64.
[7] S.M.L. Nai, J. Wei, M. Gupta, J. Alloys Compd. 473 (2009) 100–106.
[8] P. Liu, P. Yao, J. Liu, J. Alloys Compd. 470 (2009) 188–194.
[9] S. Kikuchi, M. Nishimura, K. Suetsugu, T. Ikari, K. Matsushige, Mater. Sci. Eng. A 319–321 (2001) 475–479.
[10] Y. Ding, C.Q. Wang, Y.H. Tian, M.Y. Li, J. Alloys Compd. 428 (2007) 274–285.
[11] F. Ochoa, J.J. Williams, N. Chawla, J. Electron. Mater. 32 (2003) 1414–1420.
[12] C. Wei, Y.C. Liu, Z.M. Gao, R.L. Xu, K. Yang, J. Alloys Compd. 468 (2009) 154–157.
[13] F. Lang, H. Tanaka, O. Munegata, T. Taguchi, T. Narita, Mater. Char. 54 (2005) 223–229.
[14] H.T. Ma, J.C. Suhling, J. Mater. Sci. 44 (2009) 1141–1158.
[15] T.Y. Lee, W.J. Choi, K.N. Tu, J. Mater. Res. 17 (2002) 291–301.
[16] D.Q. Yu, L. Wang, J. Alloys Compd. 458 (2007) 542–547.
[17] A. Zribi, A. Clark, L. Zavalij, D. Borgesem, E.J. Cotts, J. Electron. Mater. 30 (2001) 1157–1164.
[18] C. Yu, H. Lu, S.M. Li, J. Alloys Compd. 460 (2008) 594–598.
[19] M. He, Z. Chen, G.J. Qi, Acta Mater. 52 (2004) 2047–2056.
[20] W. Yang, R.W. Messier, L.E. Felton, J. Electron. Mater. 23 (1994) 765–772.
[21] Q.S. Zhu, Z.F. Zhang, J.K. Shang, Z.G. Wang, Mater. Sci. Eng. A 435–436 (2006) 588–594.
[22] Q.K. Zhang, H.F. Zou, Z.F. Zhang, J. Electron. Mater. 38 (2009) 852–859.
[23] M. Kerr, N. Chawla, Acta Mater. 52 (2004) 4527–4535.
[24] P. Sun, C. Andersson, X.C. Wei, Z.N. Cheng, D.K. Shangguan, J.H. Liu, J. Alloys Compd. 437 (2007) 169–179.
[25] C. Andersson, P. Sun, J.H. Liu, J. Alloys Compd. 457 (2008) 97–105.
[26] F.L. Zhu, H.H. Zhang, R.F. Guan, S. Liu, Microelectron. Eng. 84 (2007) 144–150.
[27] I. Shohji, T. Yoshida, T. Takahashi, S. Hioki, Mater. Sci. Eng. A 366 (2004) 50–55.
[28] A.A. El-Daly, Y. Swilem, A.E. Hammad, J. Alloys Compd. 471 (2009) 98–104.
[29] O. Fouassier, J.M. Heintz, J. Chazelas, P.M. Geffroy, J.F. Silvain, J. Appl. Phys. 100 (2006) 043519.
[30] H. Mavoori, J. Chin, S. Vaynman, B. Moran, L. Ker, M. Fine, J. Electron. Mater. 26 (1997) 783–790.
[31] J. Glazer, J. Electron. Mater. 23 (1994) 693–700.
[32] M. Dao, N. Chollacoop, K.J. Van Vliet, T.A. Venkatesh, S. Suresh, Acta Mater. 49 (2001) 3899–3918.
[33] X. Deng, N. Chawla, K.K. Chawla, M. Koopman, Acta Mater. 52 (2004) 4291–4303.
[34] Y.H. Lee, H.T. Lee, Mater. Sci. Eng. A 444 (2007) 75–83.
[35] J. Zhao, C.Q. Cheng, L. Qi, C.Y. Chi, J. Alloys Compd. 473 (2009) 382–388.